ISBN 978-92-990073-5-8

3rd Imeko TC13 Symposium on Measurements in Biology and Medicine
"New Frontiers in Biomedical Measurements"
April 17-18, 2014, Lecce, Italy

AUTOMATIC SEGMENTATION OF VERTEBRAL INTERFACES IN ECHOGRAPHIC IMAGES

M. Aventaggiato[1], F. Conversano[2], E. Casciaro[2], R. Franchini[2], A. Lay-Ekuakille[3], M. Muratore[4], and S. Casciaro[2]

[1]Echolight S.r.l., Lecce , Italy; [2]National Research Council, Institute of Clinical Physiology, Lecce, Italy; [3]University of Salento, Department of Innovation Engineering, Lecce, Italy; [4]O.U. of Rheumatology, Galateo Hospital, San Cesario di Lecce, ASL-LE, Lecce, Italy.

Mailing address: c/o Campus Universitario Ecotekne (Ed. A7), via per Monteroni, 73100 Lecce, Italy,

Abstract: Quantitative ultrasound (QUS) methods for osteoporosis diagnosis potentially provide information about the bone quality and its elastic properties. In this context, a novel ultrasound-based method for spinal and femoral densitometry was developed by our research group. In order to maximize its accuracy, it is very important to properly detect the bone interfaces that will be analyzed as regions of interest (ROIs). A fully automatic segmentation algorithm was developed to select lumbar vertebral interfaces in echographic images and its actual accuracy was assessed in the present work by means of a visual checking carried out by an expert operator. Abdominal US scans of lumbar spine (from L1 to L4) were performed on 100 female subjects (60.5±3.0 years old) with different ranges of body mass index (BMI) (25.8±4.6 kg/m^2). During each US scan, 100 frames of radiofrequency (RF) data were stored on a PC hard disk for offline analysis. The operator scanned each vertebra, moving the probe to the next vertebra after 20 seconds. For each acquired RF data frame, the implemented algorithm generated a sectorial echographic image and, if a vertebral interface was detected, it was highlighted on the saved image. The validation procedure was performed by an expert operator previously trained to detect the "optimal" vertebral interfaces for osteoporosis diagnosis. Results showed that the segmentation algorithm had a high specificity (93.4%), which reached its maximum on subjects with BMI < 25 kg/m^2 (94.2%), thus avoiding the selection of false vertebral interfaces and allowing a good accuracy of osteoporosis diagnosis.

Keywords: ultrasound imaging; automatic segmentation; vertebra; osteoporosis.

1. INTRODUCTION

In order to effectively manage and prevent osteoporosis, suitable techniques for population screenings and early diagnosis would be needed. Current methods for osteoporosis diagnosis are based on the application of either X-rays or ultrasound (US) techniques. The most commonly used X-ray based method is DXA (dual X-ray absorptiometry), which allows the quantification of bone mineral density (BMD). However, because of ionizing radiation employment and large size of the equipment, with its high costs, DXA is not appropriate in primary healthcare or as a screening tool, although it represents the current gold standard because of its accuracy and repeatability [1,2]. Quantitative ultrasound (QUS) methods for osteoporosis assessment have shown the potential to determine the bone quality and provide information not only about bone density but also about its structure and elastic properties [3,4]. Although they are not as accurate and repeatable as DXA, QUS techniques are less expensive and do not use ionizing radiation and, moreover, they are faster, easier to use and more portable [1].

In this context, an innovative US device was developed in Lecce (Italy) within the ECHOLIGHT Project through a collaboration between CNR-IFC and Echolight srl. This is a biomedical diagnostic system able to assess the bone status by means of a novel non-invasive technique based on US waves directly investigating the central skeleton sites, i.e. lumbar vertebrae and proximal femur [5]. The system consists of specific hardware and software components that were designed to process the radiofrequency (RF) signals acquired during an echographic scan of the target anatomical site.

In order to assess the osteoporosis status of lumbar spine, for instance, the user performs an echographic scan that starts on the L1 vertebra and ends on the L4 by maintaining the US probe on the subject's abdomen as close and parallel as possible to the sagittal plan. The US waves emitted from the probe pass through different tissues (such as skin, fat, muscles and intestine) before reaching the target bone interface. The tissue characteristics (such as, thickness, density, morphology, etc.) are different from subject to subject and, therefore, it is not possible to predict the vertebral interface position without analyzing the specific echographic image. Furthermore, other interfaces preceding vertebral surfaces in the image, such as abdominal aorta walls, make more difficult the implementation of an automatic segmentation algorithm. For these reasons, classical algorithms used for bone morphometry [6-8] are typically ineffective, because the algorithm should be able to: 1) segment all the possible vertebral interfaces present

ISBN 978-92-990073-5-8

within the frame; 2) choose the actual vertebral interface among all those resulting from the previous step by means of a ranking method. In order to make the vertebral interface identification automatic and operator-independent, a dedicated algorithm was developed by our research group.

In this work, we validated the implemented segmentation algorithm through a detailed and objective assessment of its actual accuracy when applied to real cases acquired in a clinical context.

2. METHODS

Abdominal ultrasound scans of lumbar spine were performed on 100 female subjects (60.5±3.0 years old) with different ranges of body mass index (BMI) (25.8±4.6 kg/m^2) employing the mentioned US device, equipped with a 3.5 MHz echographic convex probe. For each subject, age, height, and weight data were collected. During the US scan, 100 frames of RF data were sampled at 40 MHz and stored on a PC hard disk for offline analysis. The operator kept the probe on the subject's abdomen as close and parallel as possible to the sagittal plan and scanned each vertebra, moving the probe to the next vertebra after hearing the acoustic signal generated by the system every 20 seconds (i.e., the total scan time was 80 s/patient).

For each acquired RF data frame, the implemented algorithm generated a sectorial echographic image and, if a vertebral interface was detected and confirmed through the procedure described later, a bold red line was added on the image to highlight the interface, as shown in Fig. 1. Technical details about the automatic segmentation, the convex image generation, and the expert operator validation procedures are reported below.

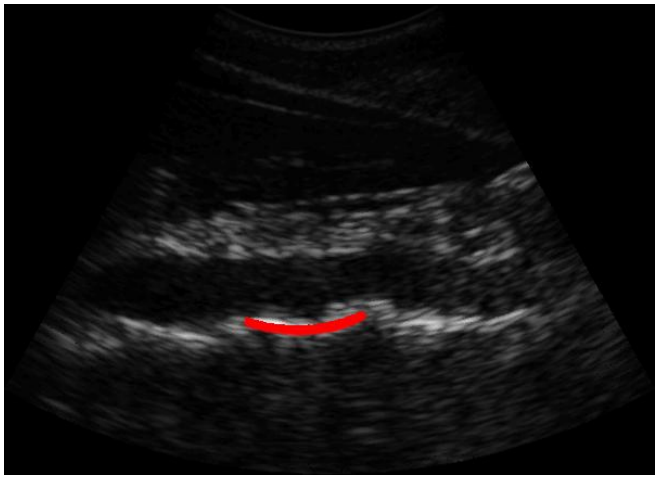

Figure 1. Segmentation of the "optimal" vertebral interface performed by the automatic algorithm. Other vertebral interfaces were present within the frame, but the automatic algorithm selected the "optimal" one: best position and best geometric properties.

Segmentation algorithm: As shown in the flow chart reported in Fig. 2, for each acquired frame, the RF signals were filtered by a band-pass Finite Impulse Response (FIR) filter with cutting frequencies at 1.0 MHz and 2.5 MHz, respectively. In this way, the amplitude of the noise possibly present at the low and high frequencies was reduced, emphasizing the contributions of those signal components that were able to pass through depth tissues and be scattered back towards the probe. At a later stage, the absolute value of the obtained signal was calculated and filtered with a low-pass FIR filter with cutting frequency at 100 kHz.

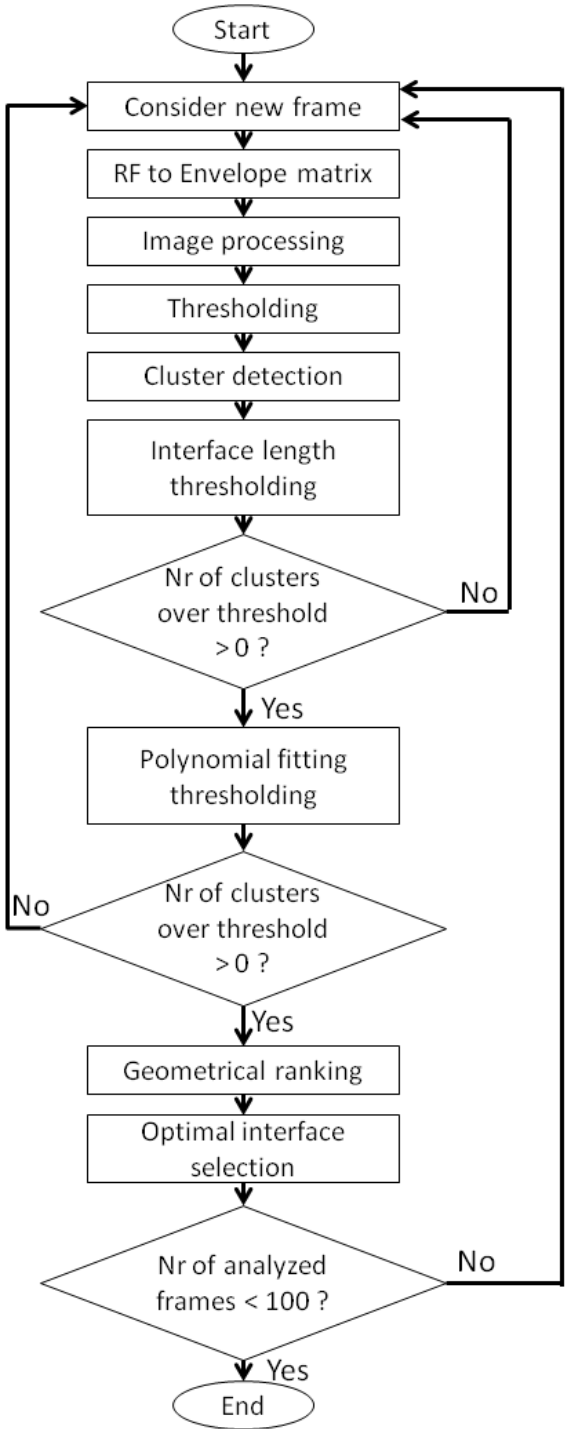

Figure 2. Flow chart of the segmentation algorithm. The corresponding image processing steps are reported in Fig. 4.

The resulting signal was the envelope of the original RF signal (see Fig. 3), which was organized as a matrix called Env_mat and having size $N_{pix} * N_{lines}$, where N_{pix} was the number of samples per scan line, which depends on scan

ISBN 978-92-990073-5-8

depth, and N_{lines} was the number of scan lines (see Fig. 4A). At this step, Env_mat was normalized between 0 and 255 and sent to the convex image generation algorithm (see section below).

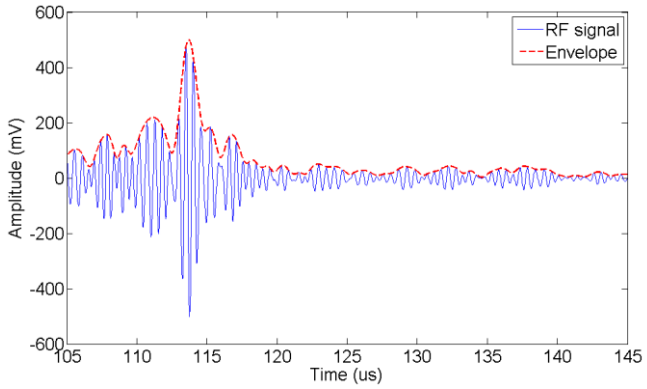

Figure 3. An example of RF signal (continuous blue line) and the corresponding envelope (dashed red line).

Since vertebral interfaces were expected to be in the central area of the frame, a power-like compensation designed to attenuate the upper and lower image portions was applied to the envelop matrix. In order to do this, we used a matrix called Exp_tgc, having $N_{pix} * N_{lines}$ elements and defined as:

$$Exp\_tgc[i,j] = \begin{cases} \frac{i}{0.3\ N_{pix}};\ if\ i \leq 0.25\ N_{pix} \\ \frac{i+0.2\ N_{pix}}{0.5\ N_{pix}};\ if\ 0.25\ N_{pix} < i \leq 0.55\ N_{pix} \\ 1.5;\ if\ 0.55 < i \leq 0.75\ N_{pix} \\ \frac{1.4N_{pix}-i}{0.5N_{pix}};if\ 0.75\ N_{pix} < i \leq 0.9\ N_{pix} \\ \frac{N_{pix}-\ i}{0.1\ N_{pix}};\ if\ 0.9\ N_{pix}\ < i \leq N_{pix} \end{cases} \quad (1)$$

Each [i,j] element of Env_mat was raised at the power represented by the [i,j] element of Exp_tgc, obtaining the matrix Env_mat2 (see Fig. 4B):

$$Env\_mat2[i,j] = Env\_mat[i,j]^{Exp\_tgc[i,j]} \quad (2)$$

Then, Env_mat2 matrix was element by element multiplied by two luminosity masks ($Mask_1$ and $Mask_2$) that emphasized the central image portion in the horizontal and in the vertical direction, respectively (see Fig. 4C). $Mask_1$ and $Mask_2$ were defined as:

$$Mask_1[i,j] = \begin{cases} \frac{2j+N_{lines}-4}{2N_{lines}-4};\ if\ 1 \leq j \leq \frac{N_{lines}}{2} \\ \frac{3N_{lines}-2-2j}{2N_{lines}-4};if\ \frac{N_{lines}}{2}+1 \leq j \leq N_{lines} \end{cases} \quad (3)$$

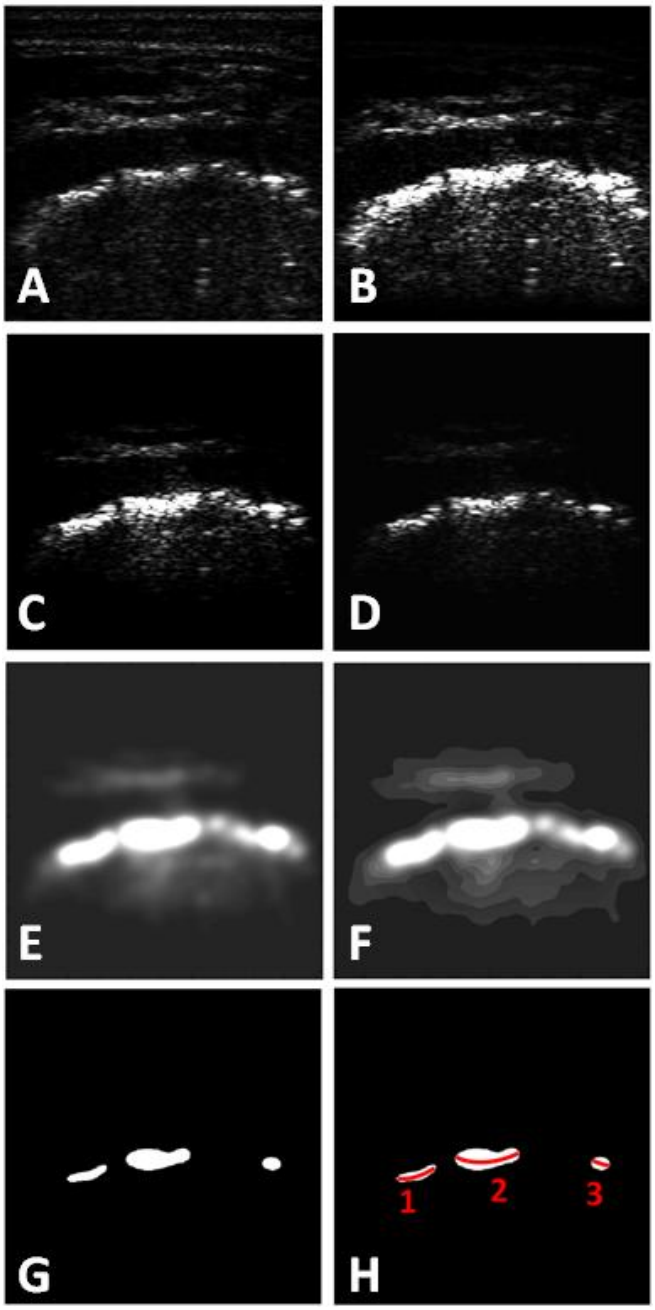

Figure 4. Image processing for the detection of possible vertebral interfaces. **A)** Image simply obtained from the envelope of the acquired RF signal. **B)** Image obtained after the application of eq. (2). **C)** Image resulting from the application of luminosity masks as defined in eq. (3) and eq. (4). **D)** Contrast optimization by using the contrast-limited adaptive histogram equalization. **E)** Image obtained after the application of the 2D Gaussian blurring filter. **F)** Image resulting from the second contrast optimization (i.e. second application of the contrast-limited adaptive histogram equalization). **G)** Thresholded black and white image with vertebral interface areas in white. **H)** Vertebral interfaces obtained by interpolating the local maximum of each scan line with a 2nd order polynomial. Possible vertebral interfaces shown in H) are ranked in order to select the optimal one (which in this case was the interface numbered as 2).

ISBN 978-92-990073-5-8

$$Mask_2[i,j] = \begin{cases} 0.5;\ if\ i \le 0.18\ N_{pix} \\ \frac{i+0.14N_{pix}}{0.64N_{pix}};\ if\ 0.18\ N_{pix} < i \le 0.5\ N_{pix} \\ 1;\ if\ 0.5 < i \le 0.6\ N_{pix} \\ \frac{1.2N_{pix}-i}{0.6N_{pix}};\ if\ 0.6\ N_{pix} < i \le 0.9\ N_{pix} \\ 0.5;\ if\ 0.9\ N_{pix} < i \le N_{pix} \end{cases} \quad (4)$$

The resulting matrix was rescaled to 512x512 elements by means of the "Nearest neighbor interpolation", normalized between 0 and 1 and processed with several steps of image processing, hereinafter described. The image contrast was optimized through the contrast-limited adaptive histogram equalization (i.e., first, the image was divided in 64 identical rectangular regions, then the histogram of each region was equalized and the neighboring region were combined using bilinear interpolation to eliminate artificially induced boundaries), as shown in Fig. 4D. Afterwards, the image was filtered by using a two dimensional low-pass Gaussian filter (size=50x50 and SD=5; see Fig. 4E) and the contrast was enhanced again by means of the adaptive histogram equalization (see Fig. 4F). Finally, the image was thresholded (threshold value = 0.95) to become a binary matrix (see Fig. 4G). In order to have an unambiguous correspondence between the image and the RF and envelope matrixes, the dimensions of the image matrix were restored at $N_{pix} * N_{lines}$ elements. As shown in Fig. 4H, each group of white pixels present in the image was identified and labeled. The length of each cluster was measured and if it was outside the range 20–45 mm the cluster was discarded from the subsequent evaluations. In order to take into account the shape of the analyzed interfaces, for each cluster, the coordinates of the local maxima of the corresponding envelope of each scan line were calculated and interpolated by a 2nd order polynomial and, then, clusters that presented the absolute value of the first polynomial coefficient higher than 0.3 were discarded. If no clusters presented a length inside the range, the frame was discarded and a new frame was considered, otherwise if more than one cluster was inside the length and shape specifics, they were ranked by means of the following criteria: A) *length*: 2 points were assigned to the longest, 1 point to the second one; B) *average vertical thickness*: 2 points to the thinnest, 1 point to the second one; C) *vertical position*: 2 points to the closest to the image center along the vertical direction and 1 point to the second one; D) *lateral position*: 2 points were assigned to the cluster that was closest to the image center along the horizontal direction, 1 point to the second one. In the end, the cluster with the highest score was selected as the image area where the vertebral interface actually was and the 2nd order polynomial previously calculated was send to the "image generation process" to highlight in red the vertebral interface on the corresponding sectorial image.

Convex image generation: In order to obtain the echographic images for the validation procedure, the Env_mat envelope matrix obtained from each frame through the procedure described in the previous section was processed following these steps: A) Env_mat was element by element multiplied by $Mask_1$ and $Mask_2$ calculated as shown in eq. (3) and eq. (4); B) the resulting matrix was filtered by a 2D Gaussian filter (size=10x10; SD=1) in order to attenuate the possibly present high frequency noise; C) the matrix was transformed into a sectorial image by taking into account the radius and field of view of the probe; D) the image was compressed to an 8-bit image; E) if the segmentation algorithm detected a vertebral interface, it was represented as a bold red line on the convex image; F) the image was saved in Portable Network Graphics (PNG) format.

Expert operator validation procedure: The validation procedure was performed by an expert operator that had been previously trained to detect the "optimal" vertebral interfaces for osteoporosis diagnosis. For each analyzed subject, the expert operator visualized each frame and classified it as true positive (if the highlighted interface was an optimal vertebral interface), true negative (if the image of the frame did not represent any vertebral interface useful to the osteoporosis analysis), false positive (if the highlighted interface was not a vertebral interface or was not the optimal one among those present), or false negative (if an optimal vertebral interface was present, but it was not detected by the algorithm). The accuracy of the segmentation algorithm was calculated in terms of sensitivity and specificity as:

$$sensitivity = \frac{True\ Positives}{True\ Positives + False\ negatives} \quad (5)$$

$$specificity = \frac{True\ negatives}{True\ negatives + False\ positives} \quad (6)$$

3. RESULTS

The results of the validation procedure carried out by the expert operator by checking the sectorial echographic images generated by the implemented algorithm are reported in Table 1. Results are shown in terms of true positive, true negative, false positive and false negative segmentations and they are grouped for all subjects and for subjects with different BMI ranges: BMI <25 kg/m^2, 25 kg/m^2 ≤ BMI ≤ 30 kg/m^2, and BMI > 30 kg/m^2.

Table 1: Results of the expert operator validation of the segmentation algorithm.

	BMI ranges (kg/m^2)			
	[0, +∞[	**[0, 25[**	**[25, 30]**	**]30, +∞[**
Nr of subjects	100	53	32	15
Nr of frames	10'000	5'300	3'200	1'500
True positive	41.2%	44.1%	39.9%	33.4%
True negative	37.8%	32.3%	41.3%	49.8%
False positive	2.7%	2.0%	3.1%	4.0%
False negative	18.4%	21.6%	15.7%	12.8%
Sensitivity	**69.1%**	67.1%	71.8%	72.3%
Specificity	**93.4%**	94.2%	93.0%	92.6%

ISBN 978-92-990073-5-8

4. DISCUSSION

The algorithm described in this work was developed and tuned in order to select the vertebral interface present in an echographic image by means of the image segmentation procedure presented above.

Since, once a vertebral interface was detected by the algorithm, its position was provided to the osteoporosis diagnosis algorithm separately developed within the mentioned research project [5], it was important to minimize the number of false positive vertebral interfaces in order to optimize the osteoporosis diagnosis. This goal was achieved by maximizing the segmentation specificity, calculated through eq. (6), although there was a corresponding decrease in sensitivity, calculated through eq. (5). We started segmentation tests setting the algorithm sensitivity close to 100%, but the number of validated frame was so high to request long computational time without any advantages in result accuracy, which, on the other hand, was affected by the decreased specificity. As shown in Table 1, when using the finally determined tuning of the segmentation algorithm, the sensitivity of the algorithm estimated on 100 subjects with different age (60.5 ± 3.0 years old) and BMI (25.8 ± 4.6 kg/m^2) was 69.1% and the specificity was 93.4%. It is also important to note that just the 2.7% of acquired frames were detected as false positives, resulting in a very low exposure of osteoporosis diagnosis to a fault condition. For different BMI ranges, obtained results showed that, for increasing values of BMI, the number of frames actually containing an "optimal" vertebra (i.e., true positives + false negatives) decreased from 65.7% (BMI < 25 kg/m^2) to 46.2 % (BMI > 30 kg/m^2), probably because of the increasing thickness of tissues between the probe and the scanned vertebra. Similarly, the rate of false positives doubled from 2.0% (BMI ≤ 25 kg/m^2) to 4.0% (BMI > 30 kg/m^2) and the specificity decreased from 94.2% (BMI < 25 kg/m^2) to 92.6% (BMI ≤ 30 kg/m^2), while the sensitivity of the algorithm correspondingly increased by 5.2%, going from 67.1% (BMI < 25 kg/m^2) to 72.3% (BMI > 30 kg/m^2).

4. CONCLUSIONS

Quantitative ultrasound (QUS) methods for osteoporosis diagnosis potentially assess the bone quality and its elastic properties. In order to increase their accuracy, because of the univocal relationship between the ultrasound signal used for the diagnosis and the image employed for the segmentation, it is very important to properly detect the vertebral interfaces that will be analyzed as region of interest. Therefore, in order to avoid affecting the osteoporosis diagnosis by selecting false vertebral interfaces, it is essential to maximize the segmentation specificity, in case also at the expenses of sensitivity.

In this work, we developed a segmentation algorithm able to detect vertebral interfaces in echographic images generated by processing the raw RF ultrasound signal. When more than one vertebral interface was present, the algorithm was able to rank them and select the optimal one, i.e. the one with properties that could provide a more accurate osteoporosis diagnosis.

The implemented segmentation algorithm was very specific (93.4%) on the 10'000 frames analyzed, and only in 2.7% of them the expert operator identified an error. The segmentation algorithm provided the best performances on subjects with BMI < 25 kg/m^2, obtaining a specificity of 94.2%.

In order to further optimize the segmentation algorithm performances, future works will be focused to tune the algorithm sensitivity and specificity in function of BMI to equalize the results independently of the tissue thickness between the probe and the vertebral interface.

5. ACKNOWLEDGEMENTS

This work was partially funded by FESR P.O. Apulia Region 2007-2013 – Action 1.2.4 (grant n. 3Q5AX31: ECHOLIGHT Project).

6. REFERENCES

[1] P. Pisani, M. D. Renna, F. Conversano, E. Casciaro, M. Muratore, E. Quarta, M. Di Paola, S. Casciaro, "Screening and Early Diagnsosis of Osteoporosis through X-ray and Ultrasound Based Techniques," World Journal of Radiology, vol. 5, no. 11, pp. 398-410, November 2013.

[2] J. A. Kanis, E. V. McCloskey, H. Johansson, C. Cooper, R. Rizzoli, J.-Y. Reginster, "European Guidance for the Diagnosis and Management of Osteoporosis in Postmenopausal Women," Osteoporosis International, vol. 24, pp. 23-57, 2013.

[3] J. J. Kaufman and T. A. Einhorn, "Ultrasound Assessment of Bone," Journal of Bone and Mineral Research, vol. 8, pp. 517-525, 1993.

[4] C. F. Njeh, C. M. Boivin, C. M. Langton, "The Role of Ultrasound in the Assessment of Osteoporosis: A Review," Osteoporosis International, vol. 7, pp. 7-22, 1997.

[5] F. Conversano, E. Casciaro, R. Franchini, G. Soloperto, A. Greco, S. Casciaro, E. Quarta, L. Quarta, M. Muratore, "A New Ultrasonic Method for Lumbar Spine Densitometry," in Proc. of IEEE International Ultrasound Symposium (IUS), pp. 1809-1812, 2013.

[6] G. Guglielmi, D. Diacinti, C. Van Kuij, F. Aparis, C. Kresta, J. F. Adams, T. M. Link, "Vertebral Morphometry: Current Methods and Recent Advances", European Journal of Radiology, vol. 18, pp. 1484-1496, 2008.

[7] D. Štern, V. Njagulj, B. Likar, F. Pernuš, T. Vrtovec, "Quantitative Vertebral Morphometry based on Parametric Modeling of Vertebral Bodies in 3D," Osteoporosis International, vol. 24, no. 4, pp. 1357-1368, April 2013.

[8] Y. Zeng, M. S. Nixon, R. Allen, "Automated Segmentation of Lumbar Vertebrae in Digital Videofluoroscopic Images", in IEEE Transactions on Medical Imaging, vol. 23, no. 1, pp. 45–52, January 2004.